Universidade Nova de Lisboa
Faculdade de Ciências e Tecnologia
Departamento de Conservação e Restauro

# Archaeological Roman Glasses

## Comparative characterisation by non-destructive analytical techniques

**Paula Alexandra Pinto Rodrigues**

Dissertation presented in fulfilment of the requirements for the
Master's degree in Conservation and Restoration

Supervisor
**Professor Doctor Rui C. da Silva**
Instituto Tecnológico e Nuclear

Co-Supervisors

**Doctor Luís C. Alves**
Instituto Tecnológico e Nuclear

**Professor Doctor Márcia Vilarigues**
Universidade Nova de Lisboa

Examiner
**Doctor M. Fátima Araújo**
Instituto Tecnológico e Nuclear

President of the Jury
**Professor Doctor Ana Maria Ramos**
Universidade Nova de Lisboa

February 2011

# Archaeological Roman Glasses

## Comparative characterisation by non-destructive analytical techniques



Paula Alexandra Pinto Rodrigues

Faculdade de Ciências e Tecnologia – Universidade Nova de Lisboa

Universidade Nova de Lisboa

**Acknowledgements**

This work and MicroFEx development were partially supported by Fundação para a Ciência e Tecnologia (FCT) and POCI 2010 (co-financed by FEDER) under contract POCI/CTM/60685/2004. Thanks are due to the Museu Municipal de Arqueologia da Amadora for providing and allowing us to analyse the samples from Quinta da Bolacha, in particular in the person of its archaeologist Gisela Encarnação.

**Sumário**

As campanhas arqueológicas no sítio da *villa* Romana da Quinta da Bolacha na Amadora, Portugal, resultaram na recolha de vários tipos de materiais e objectos diferentes. Estes apontam para duas ocupações diferentes do espaço, entre os séculos III e IV d.C. De modo a definir-se materialmente esses momentos, fragmentos de vidro recolhidos em contextos associados a ambas as ocupações foram analisados não destrutivamente por técnicas de feixes de iões, nomeadamente a emissão de raios X induzida por partículas (PIXE – *Particle Induced X ray Emission*) em combinação com a emissão de raios γ induzida por partículas (PIGE – *Particle Induced Gamma Emission*) e fluorescência de raios-X (XRF – *X ray Fluorescence*). Devido ao seu deficiente estado de preservação, nomeadamente a delaminação das superfícies do vidro, os objectos museológicos não puderam sofrer amostragem ou ser analisados em vácuo, fazendo da análise em ambiente normal uma melhor opção para o seu estudo. Foram utilizados a nova linha de feixe externo, MicroFEx, acoplada ao acelerador de partículas do ITN, e o espectrómetro de micro-fluorescência de raios X, ArtTAX, pertencente ao DCR-FCT-UNL, para a produção de conjuntos satisfatórios de resultados.

A combinação das técnicas provou ser adequada no estudo deste tipo de materiais, apesar da necessidade de se efectuar alguns ajustes. Adicionalmente, a combinação das técnicas espectrométricas PIXE/PIGE *versus* XRF permitiu também estabelecer as bases para a utilização das mesmas como sendo verdadeiramente complementares, tomando partido e assentando no carácter específico de cada técnica.

O estudo permitiu determinar a ausência de correlação entre a composição dos fragmentos e os seus contextos arqueológicos de origem. Tal, por sua vez, indica que os vidros correspondentes têm uma composição comum, transversal aos diferentes períodos de ocupação. Esta conclusão encontra-se em conformidade com o que é conhecido sobre vidro Romano, cujas composições se revelaram muito uniformes entre países e ao longo dos séculos (desde o primeiro milénio até ao séc. IX d.C.). Como consequência e à luz destas descobertas, seria expectável que poucas ou nenhumas diferenças significativas fossem encontradas entre vidros de dois períodos de ocupação tão próximos na História (cerca de um século de diferença).

Palavras-chave: vidro arqueológico; não-destrutiva; XRF; PIXE; PIGE; IBA.

**Summary**

The archaeological campaigns in the site of the Roman *villa* of Quinta da Bolacha at Amadora, Portugal, provided a recollection of many different types of materials and objects. These indicate two different occupations of the space, between III and IV centuries AD. In order to materially define those moments, fragments of glass from contexts belonging to both occupations were analysed non-destructively by ion beam techniques namely Particle Induced X ray Emission (PIXE) in combination with Particle Induced Gamma Emission (PIGE) and X ray Fluorescence (XRF). Because of their poor state of conservation, namely the delamination of the glass surfaces, the museological objects could not be sampled nor analysed in vacuum, making in air analysis a better option for their study. The new external microbeam line, MicroFEx, at ITN particle accelerator, and micro-XRF spectrometer ArtTAX, at DCR-FCT-UNL, were used in order to produce satisfactory data sets.

The combination of the techniques proved to be adequate to study this kind of materials, although some adjustments need to be made. Additionally, combining the related spectrometry techniques PIXE/PIGE versus XRF allowed establishing the starting grounds for usage of these as truly complimentary, taking advantage of and building on the specific character of each technique.

The study allowed establishing that no correlation exists between the composition of the fragments and their contexts of origin. This in turn implies that the corresponding glasses have a common composition, crossing the different occupation periods. This is in agreement with what is known of Roman glasses which compositions were found to be fairly uniform across countries and across centuries (during the first millennium, to the ninth century AD). As a consequence and on the light of these findings, it is not unexpected that little or no significant differences were found between glasses from two occupation periods so close in historical time (roughly one century apart).

Keywords: archaeological glass; non-destructive; XRF; PIXE; PIGE; IBA

## Contents

Acknowledgements ..... iii

Sumário ..... v

Summary ..... vii

1. Introduction ..... 1

2. Archaeological background ..... 3

*2.1. Roman glass* ..... 3

*2.2. The* villa ..... 4

*2.3. The glass fragments* ..... 4

3. Experimental details ..... 7

*3.1. Ion Beam Analyses* ..... 7

*3.2. Energy Dispersive X Ray Fluorescence Spectrometry* ..... 8

4. Results and Discussion ..... 9

5. Conclusions ..... 25

References ..... 27

## Index of Figures

Figure 2.1: glass fragments used in the present work ..... 5

Figure 4.1: distribution of experimental results/ nominal reference compositions ratios for Corning Glass Standards (CGS) B and D. ..... 9

Figure 4.2: distribution of the sum of analysed elements and total of all concentrations, calculated by WinFund. ..... 13

Figure 4.3: K2O vs Na2O concentrations determined by IBA techniques for each of the fragments; the legend indicates the fragments' order numbers preceded by each respective context. ..... 20

Figure 4.4: elemental distribution maps of Si, Ca and Mn on glass fragment 195. ..... 22

Figure 4.5: XRF spectra of fragment 195 – superimposition of data from a corroded and non corroded area. ..... 22

**Index of Tables**

Table 2.1: typical average composition of Roman glass (expressed as weight percentages)..... 3

Table 2.2: description of the fragments used in the present work ..... 5

Table 4.1: results obtained by IBA and reference values for CGS B (wt %) ..... 10

Table 4.2: results obtained by XRF and reference values for CGS B (wt %)..... 11

Table 4.3: results obtained by IBA and XRF and reference values for CGS D (wt %) ..... 12

Table 4.4: compositions obtained by IBA for fragments from context 19 (µg/g except where % is indicated)..... 14

Table 4.5: compositions obtained by IBA for fragments from context 17 (µg/g except where % is indicated)..... 15

Table 4.6: compositions obtained by IBA for fragments from context 15 (µg/g except where % is indicated)..... 16

Table 4.7: compositions obtained by XRF for fragments from context 19 (µg/g except where % is indicated)..... 17

Table 4.8: compositions obtained by XRF for fragments from context 17(µg/g except where % is indicated)..... 18

Table 4.9: compositions obtained by XRF for fragments from context 15 (µg/g except where % is indicated)..... 19

## 1. Introduction

The glass fragments studied here belong to 3 three different archaeological contexts, at the Roman *villa* of Quinta da Bolacha: two of well determined chronology and a third one, a revolved context of unknown chronology. This study aims are twofold: *i*) it intends to contribute to the material characterisation of the occupation periods by analysing and comparing the compositions of glass fragments recovered from the different contexts. It also intends to associate the fragments of the revolved context with those of the other contexts, trying this way to determine its possible chronological attribution; *ii*) it intends to compare measurements made on the same set of samples by different but related spectrometry techniques, PIXE, PIXE/PIGE and XRF, laying the starting grounds for their usage as complimentary, taking advantage of and building on the specific character of each technique. As such, a closely related goal of this work is to ascertain a dependable process which can provide qualitative and quantitative analysis and be applicable to this particular type of objects, the archaeological/museological glass.

The unearthed glasses were in a poor state of conservation showing clear delamination of the glass surfaces, implying that these objects could not be analysed in vacuum. Given this and the museological nature of the objects analysed, sampling was also not indicated. The use of non-destructive analytical techniques was thus absolutely imperative.

The new external microbeam line in the Ion Beam Laboratory at Instituto Tecnológico e Nuclear now in use, MicroFEx, allows non-destructive and quantitative analysis in air, resorting to PIXE, PIGE and Rutherford Backscattering Spectrometry (RBS), without requiring any sampling or otherwise special preparation. The analysis by PIGE is, in this case, of vital importance since Roman glasses are normally characterised by having significant concentrations of Na which is not detected properly in normal in-air operating conditions by other non-destructive techniques.

The results of Ion Beam Analysis (IBA) should then be confronted with other existing techniques, in order to allow a critical comparison. Because IBA techniques are limited regarding the depth of penetration of the particles used as exciting radiation, XRF technique was also used for elemental analysis since primary X rays can penetrate deeper in materials making this technique less dependent on the state of the sample surface [1]. ArtTAX set-up in the Department of Conservation and Restoration (DCR) at Faculdade de Ciências e Tecnologia, Universidade Nova de Lisboa (FCT-UNL), has been in use since 2003 providing very useful and reliable data [2-4].

## 2. Archaeological background

### *2.1. Roman glass*

During Roman Empire and also through part of Middle Age, glass production was divided in two phases: primary and secondary. Primary production refers to glass production based on the fusion of its base components, the raw materials, these being, fundamentally, sand and natron. Sand would provide the network former – silica – as well as the stabiliser – lime – together with some contaminants. Natron would provide soda which acted as flux allowing the decrease of melting temperatures. Primary production of glass is now believed to have happened mainly in the Syro-Palestine region and in Egypt, where the prime matters were easier to reach and the technique of glass production had been found and perfected [5]. Some authors defend the existence of factories of raw glass also in Italy and Gallic and Spanish provinces confirming Pliny's writings [6]. The result of this first stage of glass production was then sold and distributed as ingots or chunks throughout the Empire to local workshops where secondary production took place i.e. the transformation of the ingots or chunks to finished artefacts [5].

Roman glass was, in its majority, soda-silica-lime glass. Table 2.1 shows the typical average composition of this historical material [7].

Table 2.1. Typical average composition of Roman glass (expressed as weight percentages)

| | | |
|---|---|---|
| Silica | $SiO_2$ | 67.0% |
| Soda | $Na_2O$ | 18.0 % |
| Lime | CaO | 8.0 % |
| Potash | $K_2O$ | 1.0 % |
| Magnesia | MgO | 1.0 % |
| Alumina | $Al_2O_3$ | 2.5 % |
| Iron Oxide | $Fe_2O_3$ | 0.5 % |
| Lead Oxide | PbO | 0.01 % |

Characteristically, Roman glass is considered a low magnesia type when it presents contents below 1.5 % of MgO and $K_2O$ which indicate the use of natron as source of flux. Glasses with higher contents of magnesia and potash would indicate the use of plant ashes as flux sources [8]. Prior to the beginning or middle of the I millennium BC, plant ash was the main source of flux, especially in Egypt and Mesopotamia. At this point, the use of natron became regular around the Mediterranean and in Europe, until the IX century AD, when it was replaced by soda-rich plant ash in the Islamic Near East and by potash-rich plant ash in Western Europe [6, 8].

## 2.2. *The* villa

The Roman *villa* of Quinta da Bolacha in Amadora, Portugal, was discovered in 1979 during prospection of a Roman aqueduct that had already been identified. The archaeological works, centred in Sectors I and III [9] where structures had been identified, made possible identifying sealed contexts, which are attributed to III and IV centuries AD, together with revolved contexts of uncertain dating. The excavation campaigns recovered numerous objects among which the glass fragments of the present study, which belonged to different contexts. In general, the objects unearthed from the sealed contexts and the available historical information consistently point to III and IV centuries AD as the main occupation periods of the *villa*. There is the possibility, still under study, of an earlier occupation period too, possibly dating back to I/II centuries AD. This is as yet subjected to confirmation.

The fragments analysed during this study belong to contexts identified as 19, 17 and 15, which are briefly described below.

Context 19, attributed to a 1st occupation during 2nd half of the III century/1st half of IV century, corresponds to a burnt level, where there was a fire. During this occupation, the structure corresponded to a large room of a habitation. The walls were covered with painted stuccoes and the room had a central stuccoed pillar and a drain next to the wall.

Context 17 is attributed to a 2nd occupation, after the fire, during the second half of the IV century. At this time, the room was remodelled, a wall having been built to divide it. The central pillar was destroyed and 3 more drains and a fireplace were built in that space. These new structures and the objects collected, such as *anforae*, common ceramics and *terra sigillata* recipients, indicate that the new space was used as a kitchen. The context is mainly composed of fragmented ceramic shingles, suggesting a sudden event, corresponding to the ruin phase of the space, which is ascribed to the end of the IV century.

In context 15, very fragmented archaeological materials of diverse chronologies, including Roman, were gathered. This context was formed recently and is situated exactly above the sealed Roman contexts [9].

## *2.3. The glass fragments*

The fragments studied here were chosen as the most representative of each context. Figure 2.1 displays pictures of the glass fragments where they appear identified and grouped by context.

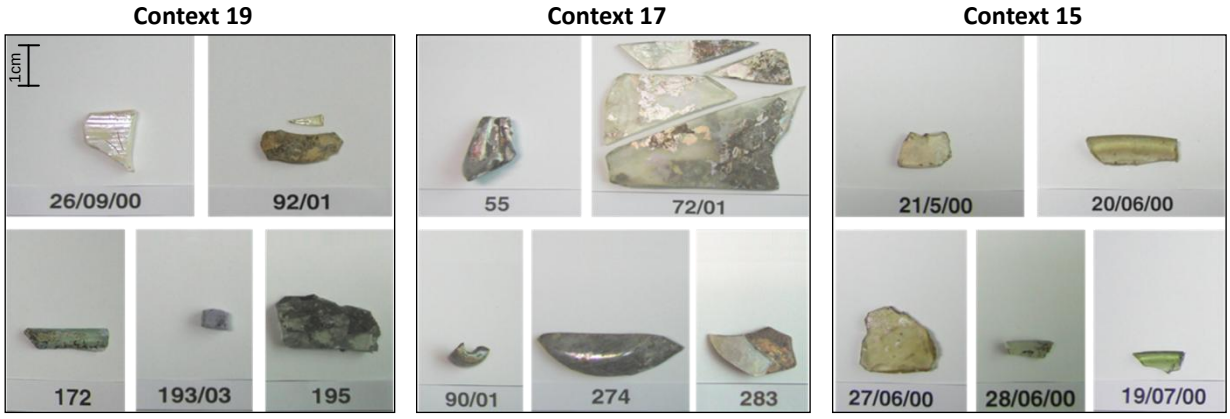


Figure 2.1: glass fragments used in the present work

Most of the fragments are of undermined typology, with exception of the blue *tesserae* – id.193/03 – and a bead fragment – id.90/01. All the fragments of undetermined typology are concave, except fragment 195 which is completely flat.

Table 2.2 resumes the objects' description.

Table 2.2: description of the fragments used in the present work

| Order number | Context | Fragment | Typology | Details |
|---|---|---|---|---|
| 1 | 19 | 26-09-00 | Undetermined | Border with *cannelures* |
| 2 and 3* | 19 | 92/01 | Undetermined | - |
| 4 | 19 | 172 | Undetermined | Border |
| 5 | 19 | 193/03 | *Tesserae* | Blue |
| 6 | 19 | 195 | Undetermined | Flat |
| 7 | 17 | 55 | Undetermined | Handle (possibly) |
| 8 | 17 | 72/01 | Undetermined | - |
| 9 | 17 | 90/01 | Bead | - |
| 10 | 17 | 274 | Undetermined | Bottom |
| 11 | 17 | 283 | Undetermined | - |
| 12 | 15 | 21-05-00 | Undetermined | - |
| 13 | 15 | 20-06-00 | Undetermined | Border |
| 14 | 15 | 27-06-00 | Undetermined | - |
| 15 | 15 | 28-06-00 | Undetermined | Border |
| 16 | 15 | 19-07-00 | Undetermined | Border |

* Larger and smaller, respectively.

## 3. Experimental details

As the recovered glass fragments displayed areas with distinctive corrosion features, care had to be taken when selecting representative zones. For bulk analysis, all the areas were chosen in order to be able to get a good flat surface with no apparent major alterations.

The objects were analysed resorting to the IBA (Ion Beam Analysis) techniques referred to above, PIXE and PIGE, and XRF.

### *3.1. Ion Beam Analyses*

Particle Induced X ray Emission (PIXE) combined with Particle Induced Gamma Emission (PIGE), were simultaneously used to determine the elemental compositions of the Roman glass pieces. Excitation of both target atomic and nuclear levels yielding characteristic X and gamma rays was provided by a 2 MeV proton beam from a 2.5 MV Van de Graaff accelerator, focused by a OM50 triplet quadrupole system onto the target, 3 mm away from a 100 nm thick $Si_3N_4$ vacuum extraction window. The 1 nA beam focused on target illuminated a spot measuring 60 × 65 $\mu m^2$. Helium gas was made to flood the analysis region with a flow of 4.5 L/min, at normal atmospheric pressure, in order to *i*) reduce energy losses of the incoming beam and attenuation of the emitted X rays, and *ii*) remove Ar, thus eliminating it as a source of spectral interference. The OM-DAQ beam steering control allowed scanning up to 1 × 1 $mm^2$ target area in synchronism with spectral data acquisition. Accurate target positioning was assured by two converging laser beams intersecting each other at the beam spot, 3 mm distant from the beam exit nozzle. A mini-video camera assists the whole procedure.

The PIXE and PIGE spectra were simultaneously collected using one 30 $mm^2$ Bruker AXS Xflash SDD (silicon drift) X rays detector of 145 eV energy resolution at 5.9 keV, and one large volume HPGe detector with 45% efficiency and 1.9 keV energy resolution (at 1.3325 MeV). The SDD detector was placed at 45º to the incoming beam direction and HPGe detector was placed at 90º.

The PIXE spectra were analysed with the AXIL [10] program for line deconvolution and DATTPIXE [11] for quantification. Although He was sprayed into the volume in front of the beam exit nozzle and SDD detector, aiming at reducing the energy losses of beam protons and attenuation of X rays, the quantification of Na was only possible through PIGE, by measuring the yield of the 440 keV gamma emission line resulting from the 23Na (p, p´γ) 23Na reaction. A rotating metallic vane was used for normalising charge collection, by measuring the X rays produced when intercepting the proton beam. Placed inside the microprobe vacuum chamber, the X rays were measured by the standard X ray Si(Li) used for microprobe analysis. The results

were compared for each sample with those obtained with Corning glass standards, allowing assessment of the quality of the detection system calibration, and control of experimental parameters.

### *3.2. Energy Dispersive X Ray Fluorescence Spectrometry*

The energy dispersive XRF was performed with ArtTAX, a portable spectrometer equipped with a SDD detector and a CCD camera and laser light diode for sample positioning. The primary X rays are produced by a Mo anode and the beam spot size is c.a. 100 µm across. This device also allows He flooding for lower Z elements detection enhancement [12].

Spectra were collected at 40 kV voltage and 600 µA current with typically 360 s acquisition time and normalised to the compositions of Corning Glass standards [13]. The XRF spectra were analysed resorting to WinAxil© software package, allowing spectra display, manipulation, deconvolution and, with WinFund© module, quantification based on fundamental parameters approach [14].

## 4. Results and Discussion

Both IBA and XRF results were analysed by resorting to the comparison with the Corning glass standards, following the same procedure as Wobrauschek et al. [15]. Tables 4.1 to 4.3 (next pages) show the quantitative results for these standards, obtained by both techniques. The plots in Fig. 4.1 display the distribution of the ratios of the experimental results to the nominal reference compositions for each of the oxides identified by the atomic number of the cation [13], allowing the quality of the analytical procedure and solutions to be evaluated.

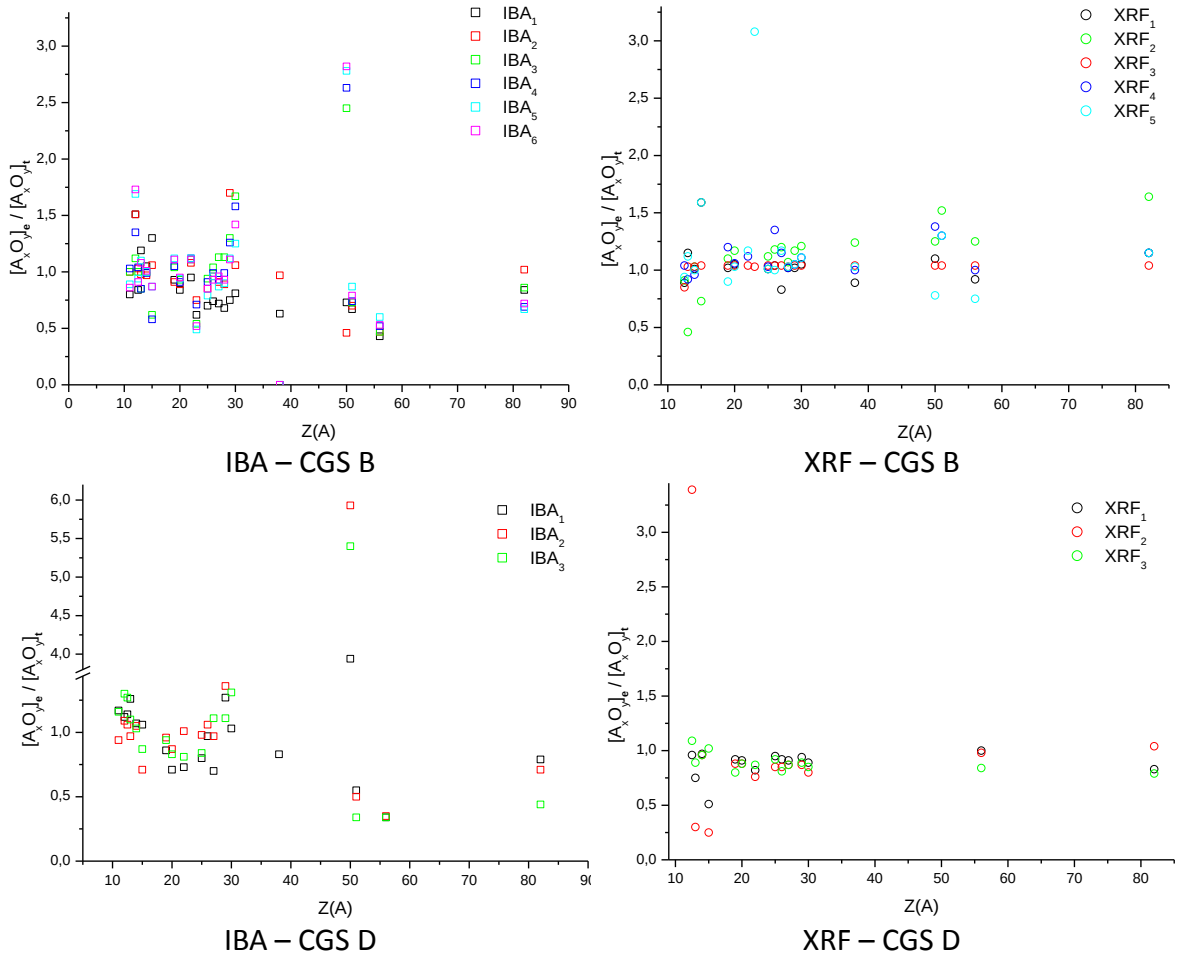


Figure 4.1: distribution of experimental results/ nominal reference compositions ratios for Corning Glass Standards (CGS) B and D.

Clearly, for both CGS B and CGS D, the scattering of the ratios is significantly higher with IBA techniques than with XRF, especially for the oxides of elements present in concentrations of the order of µg/g. As the distributions do not follow systematic patterns, these results may indicate fluctuations related to the experimental conditions, *e.g.* the state of the analysed surfaces, presenting areas free from corrosion, together with areas partially affected by corrosion to various degrees. Also the high concentrations of some metal oxides, such as tin and copper or zinc and tin/antimony seen on the IBA plots, as well as the presence of some

Table 4.1: results obtained by IBA and reference values for CGS B (wt %)

| | Corning B | | | | | | |
|---|---|---|---|---|---|---|---|
| | Reference | IBA1 | IBA2 | IBA3 | IBA4 | IBA5 | IBA6 |
| $Na_2O$ | 17 | 13.5 0.3 | 17.0 0.3 | 17.0 ± 0.2 | 17.4 ± 0.2 | 15.1 ± 0.1 | 14.6 ± 0.1 |
| MgO | 1.03 | 1.56 0.04 | 1.56 0.05 | 1.15 ± 0.03 | 1.39 ± 0.03 | 1.74 ± 0.03 | 1.78 ± 0.03 |
| $Na_2O$+MgO | *18.03* | *15.06* | *18.56* | *18.15* | *18.79* | *16.84* | *16.38* |
| $Al_2O_3$ | 4.36 | 5.17 ± 0.05 | 4.26 ± 0.06 | 3.69 ± 0.03 | 3.69 ± 0.03 | 4.81 ± 0.03 | 4.72 ± 0.03 |
| $SiO_2$ | 62.271 | 65.358 ± 0.07 | 60.32 ± 0.08 | 62.11 ± 0.08 | 61.64 ± 0.09 | 62.31 ± 0.09 | 62.855 ± 0.08 |
| $P_2O_5$ | 0.82 | 1.07 ± 0.02 | 0.87 ± 0.02 | 0.51 ± 0.01 | 0.47 ± 0.01 | 0.71 ± 0.02 | 0.71 ± 0.02 |
| $SO_3$ | - | 1.12 ± 0.02 | 0.73 ± 0.02 | 0.54 ± 0.01 | 0.56 ± 0.01 | 0.71 ± 0.02 | 0.68 ± 0.03 |
| Cl | - | 0.279 ± 0.002 | 0.055 ± 0.001 | 0.197 ± 0.003 | 0.200 ± 0.003 | 0.266 ± 0.005 | 0.245 ± 0.004 |
| $K_2O$ | 1.00 | 0.934 ± 0.003 | 0.908 ± 0.003 | 1.04 ± 0.01 | 1.047 ± 0.007 | 1.12 ± 0.01 | 1.112 ± 0.008 |
| CaO | 8.56 | 7.212 ± 0.007 | 7.655 ± 0.008 | 7.93 ± 0.02 | 7.80 ± 0.02 | 8.05 ± 0.03 | 8.15 ± 0.02 |
| $TiO_2$ | 0.089 | 0.084 ± 0.001 | 0.096 ± 0.001 | 0.099 ± 0.003 | 0.100 ± 0.003 | 0.100 ± 0.004 | 0.098 ± 0.004 |
| $V_2O_5$ | 0.036 | 0.022 ± 0.001 | 0.027 ± 0.001 | 0.019 ± 0.001 | 0.026 ± 0.002 | 0.018 ± 0.002 | 0.019 ± 0.002 |
| $Cr_2O_3$ | - | 0.009 ± 0.001 | 0.009 ± 0.001 | 0.007 ± 0.002 | 0.015 ± 0.001 | 0.007 ± 0.003 | 0.008 ± 0.003 |
| MnO | 0.25 | 0.175 ± 0.001 | 0.214 ± 0.002 | 0.234 ± 0.005 | 0.227 ± 0.005 | 0.198 ± 0.006 | 0.212 ± 0.005 |
| $Fe_2O_3$ | 0.34 | 0.251 ± 0.002 | 0.326 ± 0.002 | 0.352 ± 0.007 | 0.338 ± 0.008 | 0.325 ± 0.009 | 0.316 ± 0.008 |
| CoO | 0.046 | 0.033 ± 0.001 | 0.042 ± 0.001 | 0.052 ± 0.003 | 0.043 ± 0.003 | 0.040 ± 0.004 | 0.044 ± 0.004 |
| NiO | 0.099 | 0.068 ± 0.001 | 0.089 ± 0.002 | 0.113 ± 0.005 | 0.099 ± 0.005 | 0.090 ± 0.006 | 0.093 ± 0.005 |
| CuO | 2.66 | 2.002 ± 0.007 | 4.53 ± 0.01 | 3.453 ± 0.030 | 3.35 ± 0.03 | 2.99 ± 0.04 | 2.96 ± 0.03 |
| ZnO | 0.19 | 0.153 ± 0.002 | 0.202 ± 0.003 | 0.32 ± 0.01 | 0.30 ± 0.01 | 0.24 ± 0.02 | 0.27 ± 0.01 |
| $As_2O_5$ | - | 0.053 ± 0.004 | 0.072 ± 0.005 | 0.13 ± 0.02 | 0.177 ± 0.02 | 0.11 ± 0.02 | 0.10 ± 0.02 |
| SrO | 0.019 | 0.012 ± 0.002 | 0.018 ± 0.003 | | | | |
| $SnO_2$ | 0.04 | 0.029 ± 0.004 | 0.018 ± 0.003 | 0.098 ± 0.008 | 0.105 ± 0.007 | 0.11 ± 0.02 | 0.11 ± 0.02 |
| $Sb_2O_5$ | 0.46 | 0.308 ± 0.006 | 0.322 ± 0.006 | 0.33 ± 0.01 | 0.34 ± 0.01 | 0.40 ± 0.02 | 0.36 ± 0.02 |
| BaO | 0.12 | 0.051 ± 0.002 | 0.057 ± 0.002 | 0.057 ± 0.004 | 0.062 ± 0.004 | 0.072 ± 0.006 | 0.063 ± 0.006 |
| PbO | 0.61 | 0.51 ± 0.01 | 0.62 ± 0.02 | 0.52 ± 0.04 | 0.42 ± 0.04 | 0.41 ± 0.04 | 0.44 ± 0.04 |
| $Bi_2O_3$ | - | 0.008 ± 0.001 | 0.006 ± 0.002 | | | | |

Table 4.2: results obtained by XRF and reference values for CGS B (wt %)

| | Corning B | | | | | |
|---|---|---|---|---|---|---|
| | Reference | XRF1 | XRF2 | XRF3 | XRF4 | XRF5 |
| $Na_2O$ | 17 | | | | | |
| MgO | 1.03 | | | | | |
| $Na_2O$+MgO | *18.03* | 16.0 | 16.4 | 15.300 | 18.7 | 16.9 |
| $Al_2O_3$ | 4.36 | 5.0 ± 2.0 | 2.0 ± 0.9 | 4.490 ± 0.050 | 4.0 ± 1.0 | 4.9 ± 0.4 |
| $SiO_2$ | 62.271 | 63.0 ± 3.0 | 64.0 ± 6.0 | 64.280 ± 0.040 | 60.0 ± 2.0 | 62.0 ± 2.0 |
| $P_2O_5$ | 0.82 | 1.3 ± 0.9 | 0.6 ± 0.5 | 0.850 ± 0.030 | | 1.3 ± 0.3 |
| $SO_3$ | - | | | | | |
| Cl | - | | | | | |
| $K_2O$ | 1.00 | 1.02 ± 0.00 | 1.1 ± 0.2 | 1.037 ± 0.001 | 1.2 ± 0.2 | 0.9 ± 0.2 |
| CaO | 8.56 | 9.0 ± 0.3 | 10.0 ± 1.0 | 8.881 ± 0.002 | 9.1 ± 0.7 | 8.8 ± 0.7 |
| $TiO_2$ | 0.089 | 0.10 ± 0.02 | 0.11 ± 0.03 | 0.0924 ± 0.0002 | 0.10 ± 0.01 | 0.104 ± 0.009 |
| $V_2O_5$ | 0.036 | | | 0.037 ± 0.001 | | 0.111 ± 0.003 |
| $Cr_2O_3$ | - | | 0.017 ± 0.002 | 0.015 ± 0.001 | 0.014 ± 0.003 | 0.015 ± 0.007 |
| MnO | 0.25 | 0.252 ± 0.004 | 0.28 ± 0.03 | 0.2598 ± 0.0001 | 0.258 ± 0.003 | 0.254 ± 0.001 |
| $Fe_2O_3$ | 0.34 | 0.352 ± 0.009 | 0.40 ± 0.05 | 0.3535 ± 0.0001 | 0.46 ± 0.08 | 0.34 ± 0.06 |
| CoO | 0.046 | 0.038 ± 0.002 | 0.055 ± 0.007 | 0.0478 ± 0.0001 | 0.053 ± 0.005 | 0.054 ± 0.005 |
| NiO | 0.099 | 0.101 ± 0.002 | 0.106 ± 0.002 | 0.1029 ± 0.0001 | 0.102 ± 0.001 | 0.1026 ± 0.0001 |
| CuO | 2.66 | 2.708 ± 0.004 | 3.10 ± 0.300 | 2.7662 ± 0.0002 | 2.8 ± 0.1 | 2.8 ± 0.1 |
| ZnO | 0.19 | 0.20 ± 0.01 | 0.23 ± 0.04 | 0.1976 ± 0.0001 | 0.21 ± 0.02 | 0.21 ± 0.02 |
| $As_2O_5$ | - | | | | | |
| SrO | 0.019 | 0.017 ± 0.003 | 0.024 ± 0.001 | 0.0198 ± 0.0001 | 0.019 ± 0.001 | 0.0196 ± 0.0001 |
| $SnO_2$ | 0.04 | 0.044 ± 0.007 | 0.05 ± 0.01 | 0.0415 ± 0.0003 | 0.055 ± 0.007 | 0.031 ± 0.001 |
| $Sb_2O_5$ | 0.46 | | 0.7 ± 0.4 | 0.477 ± 0.001 | 0.6 ± 0.1 | 0.6 ± 0.1 |
| BaO | 0.12 | 0.11 ± 0.04 | 0.15 ± 0.04 | 0.1246 ± 0.0007 | 0.12 ± 0.03 | 0.09 ± 0.01 |
| PbO | 0.61 | 0.7 ± 0.1 | 1.0 ± 0.4 | 0.6344 ± 0.0002 | 0.7 ± 0.1 | 0.7 ± 0.1 |
| $Bi_2O_3$ | - | | | | | |

Table 4.3: results obtained by IBA and XRF and reference values for CGS D (wt %)

| | Corning D | | | | | |
|---|---|---|---|---|---|---|
| | Reference | IBA1 | IBA2 | IBA3 | XRF1 | XRF2 | XRF3 |
| $Na_2O$ | 1.20 | 1.41 ± 0.07 | 1.13 ± 0.05 | 1.39 ± 0.01 | | | |
| MgO | 3.94 | 4.4 ± 0.2 | 4.3 ± 0.1 | 5.13 ± 0.01 | | | |
| $Na_2O$+MgO | 5.14 | *5.81* | *5.44* | *6.52* | 4.94 | 17.40 | 5.610 |
| $Al_2O_3$ | 5.30 | 6.69 ± 0.08 | 5.13 ± 0.08 | 5.82 ± 0.02 | 4.0 ± 1.0 | 1.6 ± 0.7 | 4.700 ± 0.400 |
| $SiO_2$ | 55.46 | 59.5 ± 0.1 | 58.4 ± 0.2 | 57.12 ± 0.06 | 54.0 ± 3.0 | 53.0 ± 5.0 | 53.000 ± 2.000 |
| $P_2O_5$ | 3.93 | 4.15 ± 0.03 | 2.78 ± 0.05 | 3.42 ± 0.02 | 2.0 ± 1.0 | 1.0 ± 1.0 | 4.000 ± 1.000 |
| $SO_3$ | - | | 0.22 ± 0.02 | 0.309 ± 0.007 | | | |
| Cl | - | 0.067 ± 0.002 | 0.209 ± 0.008 | 0.243 ± 0.003 | | | |
| $K_2O$ | 11.30 | 9.72 ± 0.01 | 10.88 ± 0.05 | 10.6 ± 0.02 | 10.43 ± 0.05 | 10.0 ± 1.0 | 9.000 ± 2.000 |
| CaO | 14.80 | 10.56 ± 0.01 | 12.91 ± 0.07 | 12.22 ± 0.03 | 13.4 ± 0.4 | 13.0 ± 2.0 | 13.000 ± 1.000 |
| $TiO_2$ | 0.38 | 0.277 ± 0.003 | 0.38 ± 0.02 | 0.308 ± 0.005 | 0.31 ± 0.06 | 0.29 ± 0.07 | 0.330 ± 0.030 |
| $V_2O_5$ | - | 0.012 ± 0.001 | | | | | |
| $Cr_2O_3$ | - | | | | | | |
| MnO | 0.55 | 0.442 ± 0.003 | 0.54 ± 0.02 | 0.463 ± 0.007 | 0.52 ± 0.01 | 0.47 ± 0.06 | 0.504 ± 0.001 |
| $Fe_2O_3$ | 0.52 | 0.505 ± 0.004 | 0.55 ± 0.02 | 0.82 ± 0.01 | 0.48 ± 0.01 | 0.44 ± 0.06 | 0.420 ± 0.070 |
| CoO | 0.02 | 0.016 ± 0.001 | 0.022 ± 0.006 | 0.026 ± 0.002 | 0.021 ± 0.001 | 0.020 ± 0.003 | 0.020 ± 0.002 |
| NiO | - | 0.044 ± 0.001 | 0.08 ± 0.01 | 0.049 ± 0.003 | 0.045 ± 0.001 | 0.039 ± 0.001 | 0.042 ± 0.000 |
| CuO | 0.38 | 0.482 ± 0.005 | 0.52 ± 0.03 | 0.42 ± 0.01 | 0.356 ± 0.002 | 0.33 ± 0.03 | 0.340 ± 0.010 |
| ZnO | 0.10 | 0.103 ± 0.003 | 0.14 ± 0.02 | 0.13 ± 0.01 | 0.089 ± 0.007 | 0.08 ± 0.01 | 0.085 ± 0.008 |
| $As_2O_5$ | - | 0.067 ± 0.005 | | 0.12 ± 0.01 | | | |
| SrO | 0.057 | 0.047 ± 0.005 | | | 0.06 ± 0.01 | 0.053 ± 0.001 | 0.052 ± 0.000 |
| $SnO_2$ | 0.10 | 0.39 ± 0.01 | 0.59 ± 0.05 | 0.54 ± 0.01 | 0.09 ± 0.01 | 0.07 ± 0.02 | 0.093 ± 0.004 |
| $Sb_2O_5$ | 0.97 | 0.53 ± 0.01 | 0.48 ± 0.0 | 0.33 ± 0.01 | 2.0 ± 2.0 | 1.3 ± 0.6 | 0.800 ± 0.200 |
| BaO | 0.51 | 0.173 ± 0.003 | 0.18 ± 0.02 | 0.175 ± 0.006 | 0.51 ± 0.07 | 0.50 ± 0.06 | 0.430 ± 0.050 |
| PbO | 0.48 | 0.379 ± 0.018 | 0.34 ± 0.09 | 0.21 ± 0.03 | 0.40 ± 0.06 | 0.5 ± 0.2 | 0.380 ± 0.070 |

elements which are not specified in the reference compositions, may indicate contamination from laboratory tools used to handle the standards or the sample positioning system.

Regarding the calibration used with XRF spectra and the WinFund© software, it is possible to see in Fig. 4.2 that, by calibrating with two glass standards instead of one – even if this one is more similar in composition to the analysed samples – the sum of analysed elements comes closer to 100% for the majority of the samples. This means that the lack of a second standard, in this case, affects the values calculated by difference for the oxides of light elements, $Na_2O$ and MgO (given as $Na_2MgO_2$), as well as those of oxides not present in the standard's composition.

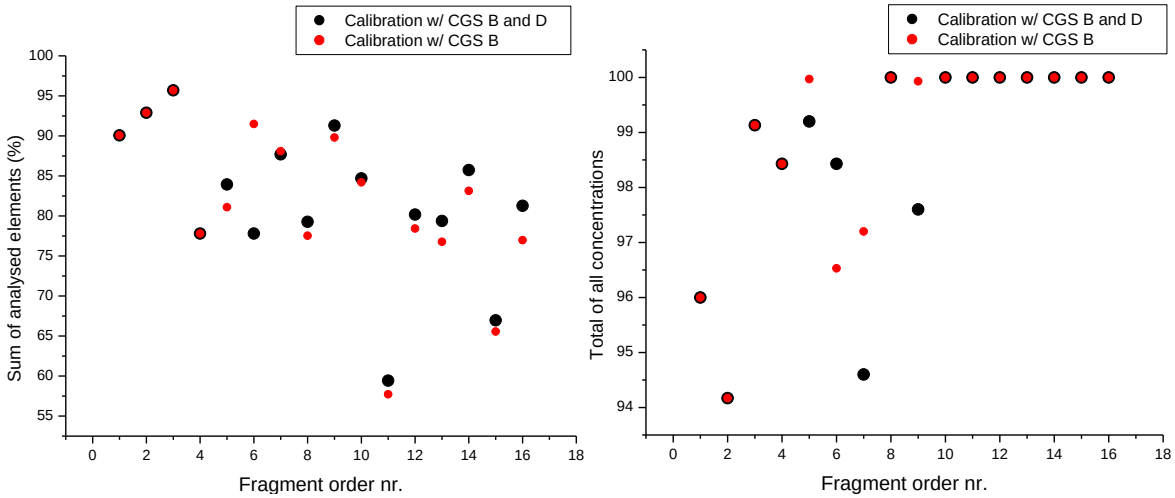


Figure 4.2: distribution of the sum of analysed elements and total of all concentrations, calculated by WinFund.

Tables 4.4 to 4.9 (next pages) summarise the compositions of the glass fragments from the different contexts, as obtained by both techniques.

Table 4.4: compositions obtained by IBA for fragments from context 19 (µg/g except where % is indicated)

| Fragment nr. | 1 | 2 | 3 | 4 | 5 | 6 |
|---|---|---|---|---|---|---|
| $Na_2O$ | 0.37% ± 0.04% | 0.8% ± 0.1% | 14.4% ± 0.7% | 17.0% ± 0.8% | 9.6% ± 0.8% | 10.9% ± 0.9% |
| MgO | 1.8% ± 0.3% | 2.0% ± 0.3% | 1.1% ± 0.2% | 1.8% ± 0.3% | 1.5% ± 0.2% | 0.8% ± 0.1% |
| $Na_2O$+MgO | *2.20%* | *2.81%* | *15.50%* | *18.74%* | *11.13%* | *11.63%* |
| $Al_2O_3$ | 9.60% ± 0.06% | 7.45% ± 0.06% | 7.63% ± 0.04% | 7.54% ± 0.05% | 7.98% ± 0.04% | 6.38% ± 0.05% |
| $SiO_2$ | 82.69% ± 0.08% | 70.21% ± 0.07% | 67.44% ± 0.06% | 64.98% ± 0.06% | 69.48% ± 0.06% | 73.23% ± 0.07% |
| $P_2O_5$ | | 1.01% ± 0.02% | 0.204% ± 0.009% | | | 0.098% ± 0.009% |
| $SO_3$ | 1654 ± 110 | 4924 ± 148 | 0.401% ± 0.008% | 0.629% ± 0.012% | 0.392% ± 0.005% | 2569 ± 79 |
| Cl | 3765 ± 26 | 0.362% ± 0.003% | 0.794% ± 0.003% | 0.823% ± 0.003% | 0.375% ± 0.002% | 0.713% ± 0.003% |
| $K_2O$ | 0.602% ± 0.002% | 1.579% ± 0.004% | 0.446% ± 0.002% | 0.675% ± 0.002% | 0.506% ± 0.002% | 0.480% ± 0.002% |
| CaO | 3.640% ± 0.006% | 14.27% ± 0.01% | 4.175% ± 0.005% | 5.186% ± 0.006% | 4.916% ± 0.005% | 5.335% ± 0.006% |
| $TiO_2$ | 416 ± 9 | 0.25% ± 0.00% | 0.518% ± 0.002% | 575 ± 9 | 304 ± 6 | 691 ± 9 |
| $V_2O_5$ | | 56 ± 8 | 0.013% ± 0.001% | | | 27 ± 5 |
| $Cr_2O_3$ | 49 ± 6 | 93 ± 9 | 61 ± 5 | 24 ± 6 | 48 ± 3 | |
| MnO | 63 ± 4 | 250 ± 7 | 1.284% ± 0.003% | 0.769% ± 0.003% | 0.221% ± 0.001% | 1.291% ± 0.004% |
| $Fe_2O_3$ | 0.386% ± 0.003% | 1.290% ± 0.005% | 1.496% ± 0.004% | 0.522% ± 0.003% | 0.728% ± 0.003% | 0.447% ± 0.003% |
| CoO | 64 ± 5 | 148 ± 8 | 101 ± 6 | 36 ± 5 | 0.158% ± 0.001% | 27 ± 5 |
| NiO | 8 ± 2 | 56 ± 7 | | | 63 ± 4 | 56 ± 5 |
| CuO | 23 ± 3 | 42 ± 4 | 58 ± 4 | 34 ± 4 | 0.229% ± 0.002% | 19 ± 3 |
| ZnO | 22 ± 3 | 44 ± 4 | 37 ± 4 | 43 ± 4 | 299 ± 8 | 60 ± 5 |
| $As_2O_5$ | 36 ± 10 | 26 ± 10 | 26 ± 7 | 41 ± 9 | 0.117% ± 0.003% | |
| Br | 73 ± 12 | | | 184 ± 15 | 18 ± 6 | |
| $Rb_2O$ | | | | | | |
| SrO | 142 ± 26 | 135 ± 24 | 243 ± 26 | 329 ± 34 | 185 ± 20 | 291 ± 31 |
| $SnO_2$ | 121 ± 32 | | | | 520 ± 22 | |
| $Sb_2O_5$ | 0.235% ± 0.006% | 0.144% ± 0.007% | | | 3.478% ± 0.007% | |
| BaO | 94 ± 12 | 383 ± 19 | 0.043% ± 0.002% | 141 ± 12 | 150 ± 7 | 217 ± 12 |
| PbO | | | | | 1212 ± 62 | |
| $Bi_2O_3$ | | | | | 22 ± 8 | |

Table 4.5: compositions obtained by IBA for fragments from context 17 (µg/g except where % is indicated)

| Fragment nr. | 7 | 8 | 9 | 10 | 11 |
|---|---|---|---|---|---|
| $Na_2O$ | 19.8% ± 1.6% | 11.5% ± 0.9% | 0.59% ± 0.09% | 24.8% ± 2.0% | 3.6% ± 0.4% |
| MgO | 1.2% ± 0.2% | 0.8% ± 0.1% | 3.4% ± 0.5% | 1.3% ± 0.2% | 1.2% ± 0.2% |
| *$Na_2O$+MgO* | *20.96%* | *12.35%* | *4.02%* | *26.10%* | *4.74%* |
| $Al_2O_3$ | 3.56% ± 0.05% | 3.87% ± 0.05% | 6.64% ± 0.07% | 2.39% ± 0.03% | 11.26% ± 0.06% |
| $SiO_2$ | 65.37% ± 0.08% | 72.57% ± 0.08% | 80.47% ± 0.10% | 64.19% ± 0.07% | 75.23% ± 0.08% |
| $P_2O_5$ | | | 0.155% ± 0.013% | | |
| $SO_3$ | 4810 ± 147 | 6752 ± 144 | 6350 ± 159 | 5684 ± 76 | 4005 ± 55 |
| Cl | 1.401% ± 0.005% | 0.914% ± 0.003% | 0.396% ± 0.003% | 1.347% ± 0.004% | 0.328% ± 0.002% |
| $K_2O$ | 0.357% ± 0.002% | 0.589% ± 0.002% | 0.275% ± 0.002% | 0.237% ± 0.001% | 0.382% ± 0.002% |
| CaO | 6.363% ± 0.008% | 7.333% ± 0.008% | 3.696% ± 0.007% | 3.875% ± 0.006% | 6.032% ± 0.007% |
| $TiO_2$ | 584 ± 11 | 660 ± 11 | 0.412% ± 0.003% | 688 ± 10 | 1497 ± 13 |
| $V_2O_5$ | 31 ± 6 | | 59 ± 12 | | 16 ± 3 |
| $Cr_2O_3$ | | 21 ± 6 | 20 ± 7 | | 43 ± 3 |
| MnO | 1.065% ± 0.004% | 1.110% ± 0.004% | 1.837% ± 0.006% | 0.785% ± 0.003% | 0.599% ± 0.003% |
| $Fe_2O_3$ | 0.341% ± 0.003% | 0.446% ± 0.003% | 1.330% ± 0.006% | 0.392% ± 0.003% | 0.833% ± 0.004% |
| CoO | 24 ± 5 | 26 ± 5 | 73 ± 9 | 33 ± 4 | 60 ± 4 |
| NiO | | | 22 ± 5 | 9 ± 2 | 8 ± 2 |
| CuO | 12 ± 3 | 37 ± 5 | 73 ± 6 | 26 ± 3 | 18 ± 3 |
| ZnO | 75 ± 6 | 37 ± 5 | 44 ± 5 | 20 ± 3 | 18 ± 3 |
| $As_2O_5$ | 29 ± 10 | 40 ± 13 | | 16 ± 6 | |
| Br | | 28 ± 11 | | | 20 ± 7 |
| $Rb_2O$ | 38 ± 14 | | | | |
| SrO | 163 ± 30 | 411 ± 46 | 266 ± 40 | 254 ± 33 | 169 ± 28 |
| $SnO_2$ | | | | | |
| $Sb_2O_5$ | | | | | |
| BaO | 88 ± 14 | 258 ± 15 | 732 ± 28 | 110 ± 9 | 44 ± 6 |
| PbO | | | | | |
| $Bi_2O_3$ | | | 34 ± 13 | | 58 ± 13 |

Table 4.6: compositions obtained by IBA for fragments from context 15 (µg/g except where % is indicated)

| Fragment nr. | 12 | 13 | 14 | 15 | 16 |
|---|---|---|---|---|---|
| $Na_2O$ | 14.8% ± 1.2% | 15.6% ± 1.2% | 12.9% ± 1.0% | 10.6% ± 0.8% | 11.8% ± 0.9% |
| MgO | 1.0% ± 0.2% | 0.61% ± 0.09% | 1.8% ± 0.3% | 0.25% ± 0.04% | 1.0% ± 0.1% |
| *$Na_2O$+MgO* | *15.80%* | *16.20%* | *14.67%* | *10.81%* | *12.79%* |
| $Al_2O_3$ | 5.36% ± 0.03% | 3.11% ± 0.04% | 6.80% ± 0.05% | 7.03% ± 0.04% | 8.77% ± 0.04% |
| $SiO_2$ | 68.85% ± 0.06% | 70.26% ± 0.07% | 68.80% ± 0.07% | 72.46% ± 0.06% | 70.05% ± 0.06% |
| $P_2O_5$ | | | | | |
| $SO_3$ | 5745 ± 68 | 5985 ± 107 | 5505 ± 121 | 2923 ± 82 | 3713 ± 50 |
| Cl | 1.080% ± 0.003% | 0.877% ± 0.003% | 0.917% ± 0.003% | 1.307% ± 0.004% | 0.956% ± 0.003% |
| $K_2O$ | 0.738% ± 0.002% | 0.632% ± 0.002% | 0.594% ± 0.002% | 0.729% ± 0.002% | 0.751% ± 0.002% |
| CaO | 5.986% ± 0.006% | 6.306% ± 0.007% | 5.835% ± 0.006% | 6.047% ± 0.006% | 3.793% ± 0.004% |
| $TiO_2$ | 0.093% ± 0.001% | 0.102% ± 0.001% | 0.101% ± 0.001% | 366 ± 7 | 0.317% ± 0.001% |
| $V_2O_5$ | | | | 20 ± 4 | 105 ± 5 |
| $Cr_2O_3$ | | | | | 34 ± 3 |
| MnO | 0.896% ± 0.003% | 1.137% ± 0.004% | 0.958% ± 0.003% | 1.035% ± 0.003% | 0.951% ± 0.003% |
| $Fe_2O_3$ | 0.560% ± 0.003% | 0.696% ± 0.003% | 0.696% ± 0.003% | 0.205% ± 0.002% | 1.155% ± 0.003% |
| CoO | 38 ± 4 | 42 ± 6 | 56 ± 6 | 14 ± 3 | 85 ± 5 |
| NiO | 11 ± 3 | | | 12 ± 4 | 14 ± 2 |
| CuO | 49 ± 4 | 39 ± 4 | 78 ± 5 | 21 ± 3 | 45 ± 3 |
| ZnO | 45 ± 4 | 34 ± 4 | 37 ± 4 | 26 ± 3 | 50 ± 4 |
| $As_2O_5$ | 33 ± 6 | | 44 ± 10 | | |
| Br | | | | | 43 ± 6 |
| $Rb_2O$ | | | | | |
| SrO | 346 ± 30 | 489 ± 43 | 408 ± 36 | 193 ± 24 | 268 ± 24 |
| $SnO_2$ | | | | | 175 ± 19 |
| $Sb_2O_5$ | | | | | |
| BaO | 170 ± 9 | 159 ± 13 | 167 ± 13 | 142 ± 10 | 112 ± 9 |
| PbO | | | | | 49 ± 16 |
| $Bi_2O_3$ | | | | | |

Table 4.7: compositions obtained by XRF for fragments from context 19 (µg/g except where % is indicated)

| Fragment nr. | 1 | 2 | 3 | 4 | 5 | 6 |
|---|---|---|---|---|---|---|
| $Na_2O$+MgO | 5.93% | 1.25% | 3.47% | 20.63% | 15.23% | 20.63% |
| $Al_2O_3$ | 11.4% ± 1.0% | 6.3% ± 0.6% | 7.8% ± 0.7% | 9.8% ± 0.8% | 5.3% ± 0.6% | 5.3% ± 0.4% |
| $SiO_2$ | 72.3% ± 2.3% | 62.0% ± 2.0% | 72.7% ± 2.7% | 59.0% ± 2.0% | 62.0% ± 2.0% | 73.3% ± 3.0% |
| $P_2O_5$ | 0.32% ± 0.08% | 0.29% ± 0.07% | 1.0% ± 0.3% | 0.33% ± 0.09% | 0.32% ± 0.09% | 0.5% ± 0.1% |
| $SO_3$ | 70 ± 15 | 475 ± 30 | 0.25% ± 0.01% | 0.43% ± 0.02% | 0.18% ± 0.01% | 393 ± 23 |
| Cl | 245 ± 12 | 0.11% ± 0.01% | 0.67% ± 0.03% | 0.23% ± 0.01% | 0.24% ± 0.02% | 0.61% ± 0.03% |
| $K_2O$ | 1.1% ± 0.2% | 1.4% ± 0.2% | 0.50% ± 0.08% | 1.0% ± 0.2% | 0.47% ± 0.08% | 0.7% ± 0.1% |
| CaO | 4.2% ± 0.3% | 20.0% ± 1.3% | 6.9% ± 0.5% | 5.6% ± 0.4% | 6.6% ± 0.5% | 8.6% ± 0.6% |
| $TiO_2$ | 467 ± 40 | 0.23% ± 0.02% | 0.90% ± 0.08% | 600 ± 53 | 900 ± 87 | 667 ± 57 |
| $V_2O_5$ | | 160 ± 10 | 0.30% ± 0.01% | 590 ± 15 | 770 ± 20 | 0.163% ± 0.005% |
| $Cr_2O_3$ | 113 ± 5 | 49 ± 3 | 231 ± 9 | 14 ± 1 | 19 ± 1 | 30 ± 2 |
| MnO | 114 ± 1 | 488 ± 2 | 2.63% ± 0.01% | 0.705% ± 0.002% | 0.401% ± 0.002% | 1.66% ± 0.01% |
| $Fe_2O_3$ | 0.49% ± 0.08% | 1.7% ± 0.3% | 2.43% ± 0.40% | 0.50% ± 0.08% | 1.1% ± 0.2% | 0.41% ± 0.07% |
| CoO | 41 ± 4 | 117 ± 10 | 163 ± 17 | 31 ± 3 | 0.29% ± 0.03% | 40 ± 4 |
| NiO | 4.1 ± 0.2 | 12.9 ± 0.2 | 18.7 ± 0.2 | | 98 ± 3 | |
| CuO | 28 ± 1 | 48 ± 2 | 103 ± 4 | 35 ± 1 | 0.36% ± 0.01% | 20 ± 1 |
| ZnO | 54 ± 5 | 79 ± 8 | 85 ± 8 | 52 ± 5 | 433 ± 40 | 50 ± 5 |
| $As_2O_5$ | 39 ± 2 | 75 ± 3 | 22 ± 1 | | 0.15% ± 0.01% | |
| Br | 51 ± 3 | 40 ± 2 | 36 ± 2 | 124 ± 6 | 34 ± 4 | 27 ± 1 |
| SrO | 447 ± 2 | 756 ± 4 | 734 ± 4 | 498 ± 3 | 428 ± 5 | 573 ± 3 |
| $SnO_2$ | 158 ± 5 | 0.1% ± 0.4% | 220 ± 8 | 262 ± 8 | 263 ± 9 | 377 ± 10 |
| $Sb_2O_5$ | 0.24% ± 0.05% | 0.26% ± 0.05% | | | 6.7% ± 1.0% | |
| BaO | 613 ± 73 | 420 ± 50 | 0.18% ± 0.02% | 333 ± 40 | | 620 ± 77 |
| PbO | 124 ± 20 | 45 ± 8 | 137 ± 23 | 120 ± 20 | 967 ± 233 | 453 ± 77 |
| Sum of analysed elements | 90.07% | 92.90% | 95.70% | 77.80% | 83.93% | 77.80% |
| Total of all concentrations | 96.00% | 94.17% | 99.13% | 98.43% | 99.20% | 98.43% |

Table 4.8: compositions obtained by XRF for fragments from context 17(µg/g except where % is indicated)

| Fragment nr. | 7 | 8 | 9 | 10 | 11 |
|---|---|---|---|---|---|
| $Na_2O$+MgO | 6.92% | 20.70% | 6.28% | 15.30% | 40.57% |
| $Al_2O_3$ | 4.8% ± 0.4% | 4.7% ± 0.4% | 7.7% ± 0.7% | 3.8% ± 0.3% | 3.7% ± 0.3% |
| $SiO_2$ | 68.7% ± 2.3% | 62.3% ± 2.0% | 71.7% ± 2.3% | 72.0% ± 3.0% | 43.3% ± 1.7% |
| $P_2O_5$ | 500 ± 200 | 0.5% ± 0.1% | 0.9% ± 0.2% | 600 ± 200 | 0.5% ± 0.1% |
| $SO_3$ | 937 ± 47 | 710 ± 40 | 0.14% ± 0.01% | 0.11% ± 0.01% | 343 ± 27 |
| Cl | 0.90% ± 0.04% | 0.45% ± 0.02% | 0.23% ± 0.01% | 0.92% ± 0.04% | 0.47% ± 0.02% |
| $K_2O$ | 0.44% ± 0.08% | 0.6% ± 0.1% | 0.32% ± 0.05% | 0.28% ± 0.05% | 0.28% ± 0.05% |
| CaO | 9.3% ± 0.7% | 8.5% ± 0.7% | 5.4% ± 0.4% | 5.7% ± 0.4% | 7.3% ± 0.5% |
| $TiO_2$ | 837 ± 67 | 613 ± 50 | 0.53% ± 0.04% | 880 ± 70 | 0.27% ± 0.02% |
| $V_2O_5$ | 3853 ± 97 | 3487 ± 90 | 2825 ± 70 | 2810 ± 80 | 2323 ± 70 |
| $Cr_2O_3$ | 39 ± 2 | 4 ± 1 | 136 ± 6 | | 108 |
| MnO | 1.90% ± 0.01% | 1.332% ± 0.004% | 2.54% ± 0.01% | 1.169% ± 0.004% | 1.69% ± 0.01% |
| $Fe_2O_3$ | 0.49% ± 0.08% | 0.43% ± 0.07% | 1.5% ± 0.2% | 0.48% ± 0.08% | 1.2% ± 0.2% |
| CoO | 41 ± 4 | 40 ± 4 | 98 ± 9 | 32 ± 3 | 67 ± 6 |
| NiO | | | | | 28.3 ± 0.2 |
| CuO | 28 ± 1 | 38 ± 1 | 81 ± 3 | 23 ± 1 | 44 ± 2 |
| ZnO | 71 ± 7 | 51 ± 5 | 83 ± 8 | 47 ± 4 | 56 ± 5 |
| $As_2O_5$ | | | | | |
| Br | 28 ± 1 | 32 ± 1 | 30 ± 1 | 37 ± 2 | 31 ± 2 |
| SrO | 582 ± 3 | 595 ± 3 | 513 ± 3 | 506 ± 3 | 597 ± 3 |
| $SnO_2$ | 437 ± 13 | 377 ± 13 | 218 ± 8 | 219 ± 7 | 298 ± 9 |
| $Sb_2O_5$ | 145 ± 30 | 390 ± 80 | | | |
| BaO | 490 ± 60 | 603 ± 77 | 0.23% ± 0.03% | 730 ± 90 | 293 ± 40 |
| PbO | 513 ± 87 | 537 ± 83 | 467 ± 80 | 450 ± 80 | 120 ± 23 |
| Sum of analysed elements | 87,70% | 79,27% | 91,30% | 84,70% | 59,43% |
| Total of all concentrations | 94,60% | 100,00% | 97,60% | 100,00% | 100,00% |

Table 4.9: compositions obtained by XRF for fragments from context 15 (µg/g except where % is indicated)

| Fragment nr. | 12 | 13 | 14 | 15 | 16 |
|---|---|---|---|---|---|
| $Na_2O$+MgO | 19.83% | 20.63% | 14.23% | 33.03% | 18.70% |
| $Al_2O_3$ | 4.77% ± 0.40% | 5.13% ± 0.43% | 5.53% ± 0.50% | 4.10% ± 0.40% | 7.3% ± 0.6% |
| $SiO_2$ | 64.00% ± 2.00% | 63.00% ± 2.00% | 66.67% ± 2.00% | 54.00% ± 2.00% | 64.3% ± 2.0% |
| $P_2O_5$ | 800 ± 300 | 1.07% ± 0.27% | 0.70% ± 0.20% | 0.70% ± 0.20% | 0.26% ± 0.07% |
| $SO_3$ | 845 ± 40 | 1760 ± 85 | 995 ± 50 | 337 ± 23 | 880 ± 50 |
| Cl | 0.53% ± 0.03% | 0.42% ± 0.02% | 0.61% ± 0.03% | 0.50% ± 0.02% | 0.55% ± 0.03% |
| $K_2O$ | 0.52% ± 0.09% | 0.57% ± 0.09% | 0.67% ± 0.10% | 0.39% ± 0.07% | 0.46% ± 0.08% |
| CaO | 7.23% ± 0.50% | 6.87% ± 0.53% | 8.60% ± 0.63% | 5.27% ± 0.40% | 4.5% ± 0.3% |
| $TiO_2$ | 0.10% ± 0.01% | 0.11% ± 0.01% | 0.14% ± 0.01% | 297 ± 23 | 0.40% ± 0.03% |
| $V_2O_5$ | 0.46% ± 0.01% | 0.25% ± 0.01% | 0.35% ± 0.01% | 0.23% ± 0.01% | 720 ± 20 |
| $Cr_2O_3$ | 14 ± 1 | | 30 ± 2 | 19 ± 1 | 120 ± 6 |
| MnO | 1.38% ± 0.00% | 1.21% ± 0.00% | 1.55% ± 0.01% | 1.12% ± 0.00% | 1.512% ± 0.005% |
| $Fe_2O_3$ | 0.70% ± 0.10% | 0.67% ± 0.10% | 0.90% ± 0.17% | 0.18% ± 0.03% | 1.5% ± 0.2% |
| CoO | 51 ± 5 | 46 ± 4 | 68 ± 7 | 24 ± 3 | 102 ± 9 |
| NiO | 7.2 ± 0.2 | | 6.7 ± 0.2 | 8.2 ± 0.2 | 22.2 ± 0.2 |
| CuO | 71 ± 3 | 42 ± 2 | 107 ± 4 | 18 ± 1 | 49 ± 2 |
| ZnO | 52 ± 5 | 47 ± 4 | 58 ± 5 | 28 ± 2 | 60 ± 5 |
| $As_2O_5$ | | | 9 ± 1 | | 10 ± 1 |
| Br | 32 ± 2 | 26 ± 1 | 32 ± 2 | 18 ± 1 | 29 ± 1 |
| SrO | | | 833 ± 4 | | 490 ± 3 |
| $SnO_2$ | 353 ± 10 | 315 ± 10 | 387 ± 10 | 258 ± 8 | 184 ± 6 |
| $Sb_2O_5$ | 327 ± 67 | | 180 ± 40 | 430 ± 80 | |
| BaO | 563 ± 67 | 317 ± 40 | 550 ± 70 | 340 ± 43 | 637 ± 70 |
| PbO | 490 ± 83 | 337 ± 60 | 397 ± 67 | 327 ± 57 | 71 ± 13 |
| Sum of analysed elements | 80.17% | 79.37% | 85.73% | 66.97% | 81.27% |
| Total of all concentrations | 100.00% | 100.00% | 100.00% | 100.00% | 100.00% |

From simple observation of the results presented, several remarks can be made: in what concerns the $K_2O$ and $Na_2O$ contents, $K_2O$ is generally below 1%, with few exceptions which probably correspond to more corroded glass fragments, and this is consistently seen by both techniques, IBA and XRF. On the contrary, although $Na_2O$ concentrations obtained by IBA present variations from ~0.37% up to ~24.8% (cf. Fig. 2.3; XRF was totally unable to provide any values for these concentrations) the overall values – obtained by IBA and calculated by differences in XRF for the joint $Na_2O$+MgO concentrations – scatter equally through large intervals, namely 2.20-26.1% as seen by IBA vs 1.26-40.6% by XRF.

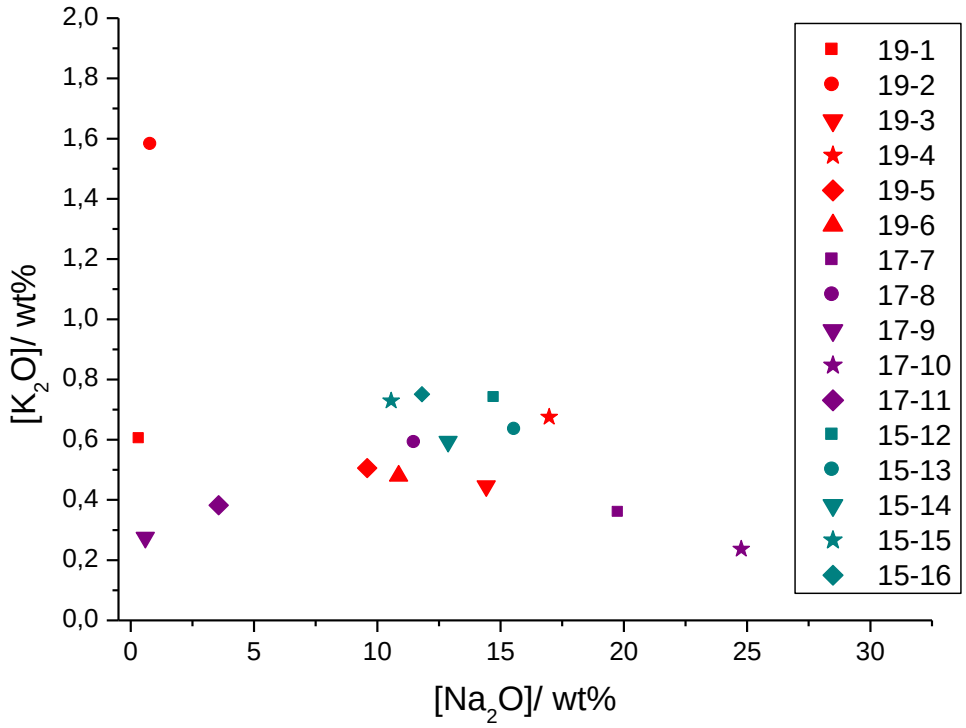


Figure 4.3: $K_2O$ vs $Na_2O$ concentrations determined by IBA techniques for each of the fragments; the legend indicates the fragments' order numbers preceded by each respective context.

Furthermore, [CaO] values vary from 3.64% to 14.27% while [MgO] stays below 2%. At this point – given the relatively low content of MgO which as such has no significant influence in the overall variation imposed by $Na_2O$ – what is surprising is the comparatively much larger scatter of results that may be inferred from XRF for $Na_2O$. This means that, as expected from Roman glasses [16], the analysed fragments are soda-lime-silica glasses showing different extents of surface corrosion, which is responsible for the removal of Na and Ca. Figure 4.3, together with the low contents of MgO presented in the presented tables, further indicate that these glasses were produced by resorting to natron as a flux [8].

It is to be noticed from inspection of the tables that all the glass fragments analysed by XRF – which probes deeper into the glasses and is thus more immune to layer alteration by corrosion

– show a consistently high content of Sr (expressed as SrO), between 400 μg/g and 800 μg/g, across contexts. Even the IBA results (that probe more shallow layers of the glasses) show consistently high contents of Sr, in the range 130 μg/g to 500 μg/g. Such results clearly indicate that Sr cannot be used as a distinctive fingerprint that might allow associating particular fragments with definite contexts in this case. They point, however, to a common source, most probably of coastal nature, either local or imported, especially if their low MgO content and noticeable absence of Zr is taken into account. In fact, according to Paynter [17], and also to Freestone [18], higher Sr concentrations, around 400 μg/g, associated with low contents of Zr ~60 μg/g [17] or low MgO contents, below 2% [18], indicate use of Mediterranean coastal sands to produce the glasses, while lower Sr values, closer to 150 μg/g, and higher concentrations of Zr, ca. 160 μg/g [17] or MgO contents above 2% [18], would suggest the use of inland sands.

Although at an earlier stage of results processing it seemed possible that grouping by similarity of composition would emerge allowing an unambiguous association between samples and contexts of origin, this proved not to be so. In spite of the apparent scattering of the results, very much influenced by the strong variation in Na contents most probably due to varying degrees and extent of glass surface corrosion, the results are fairly homogeneous in that they do not characteristically associate with any context. This is very interesting as it indicates that essentially no significant distinction exists – from the point of view of chemical/elemental composition – between samples from different contexts. As such, the reasonable conclusion that presents is that the analysed glass fragments are common to the different occupations of the archaeological site.

Fragment 193/03 from context 19 showed significant concentrations of Sb and Pb, indicating usage of opacifying agents (mixed oxides as $Ca_2Sb_2O_7$, $Ca_2Sb_2O_6$ and $Pb_2Sb_2O_7$), which are known to have been used until IV century AD [19], in agreement with the time interval of the *villa*'s occupation.

Fragment 92/01-Larger is abnormally rich in K, comparing to other samples, while low in Na contrarily to 92/01-Smaller from the same context. Therefore these two fragments should not be considered as belonging to the same original object (as opposed to what was initially accepted).

Performing beam scanning and elemental distribution mapping with IBA techniques further helped in identifying the most corroded areas of the samples.

This possibility is demonstrated for glass fragment 195 in Fig. 4.4, showing the elemental distribution maps of Si, Ca and Mn. Clearly corroded *versus* clean, non-attacked areas can be identified and distinguished through the observation of regions with reduced concentrations of

Si and Ca in correlation with corresponding regions displaying enhanced Mn contents. This is also seen by XRF in the spectra of a corroded area *versus* non-corroded area as seen in Fig. 4.5. The Mn rich regions in the PIXE maps correlate to a visible dark brown thin layer on the glass surface, probably corresponding to $MnO_2$, as the result of redeposition of Mn on the glass surface, after oxidation by atmospheric $O_2$, which in turn is subsequent to the leaching of Mn from the glass matrix [20].

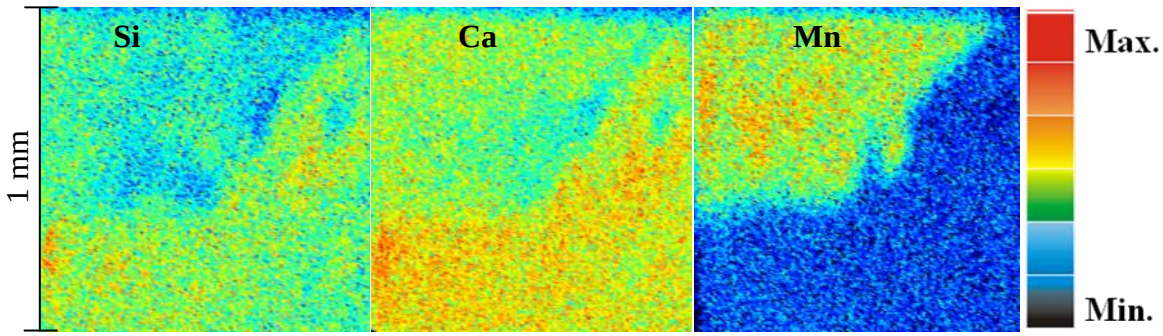


Figure 4.4: elemental distribution maps of Si, Ca and Mn on glass fragment 195.

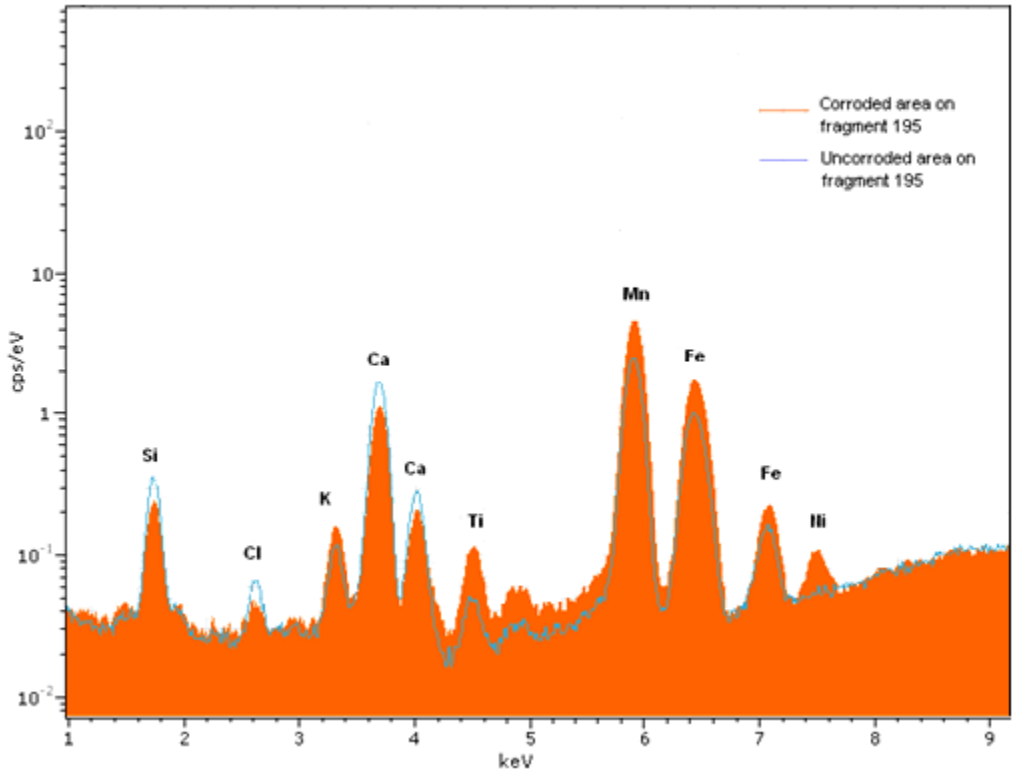


Figure 4.5: XRF spectra of fragment 195 – superimposition of data from a corroded and non corroded area.

Contact of glass with water leads to leaching of alkali and alkaline earth ions and their substitution by hydronium ions in the glass structure. This creates a hydrated layer at the

surface, causing more leaching and silica dissolution in the presence of water [21]. This mechanism may explain the low contents of both Na and K found in some of the fragments.

As expected, XRF results generally present higher contents of $SiO_2$, CaO and $K_2O$ and lower concentrations of Mn and Cl in apparent opposition to the IBA results. This can be explained by the deeper penetration of the X rays beams in the glass, and thus larger volumes of probed material.

Finally a word about processing and analysing large volumes of data as was the case of the present work and all works of similar nature.

The presently available XRF spectra processing software, although adequate for processing individual spectra or small numbers of spectra, is much less fit or adequate to handle a large number of spectra. In such cases, its use becomes difficult, even cumbersome, without proper planning and adequate knowledge of the package full possibilities. At present this is not yet an optimised process at DCR, most probably due to the fact that the necessity has not posed itself so far. Fully exploring the package's capabilities became an understandably important aim of this work, one that has also been successfully achieved. With this purpose in mind, the focus was first set in understanding the formats used for information storage and retrieval, both spectral and operational, concerning the data acquisition and analysis software. Inspecting and understanding these formats lead to realising that all pertinent experimental data is stored in block structured XML format – an ASCII format that is easily and readily machine readable and user readable – in the form of SPX files. Secondly, and equally important due to its practical implications, was the realisation that – since WinAXIL does not provide any means to directly read or accept the SPX files from the ArTAX acquisition system (or otherwise XML formatted data) – the best working format to use for conveying spectra and relevant data to WinAXIL is the SPE format. This is a well-documented block structured ASCII format, sponsored by the International Atomic Energy Agency (IAEA) and also used with previous versions of the AXIL code. Contrary to the plain ASCII format TXT commonly used at DCR, SPE formatted files store and convey relevant data to WinAXIL, in particular system times – live and real (clock) times – necessary for e.g. dead time calculations, not just the spectral data. Using these SPE format not only eliminates the need of manually entering the system times for each individual spectrum but also enables large number batch processing by means of WinAXILBatch: spectral line deconvolution and background correction can be performed unattended, automatically, for any number of spectra. Furthermore, automatic data handling also minimizes the chance for error. In order to make this possible and practical, creation of the SPE data files from the original SPX data files can also be made automatic, as a batch process. As a consequence of the needs

imposed by this work and the understanding gained about the data formats and usage, an existing batch format conversion program was implemented to accommodate batch conversion of SPX (XML) to IAEA/AXIL complying SPE format. In all, the combined use of the format conversion program and the SPE files with WinAXILBatch, allow a reduction of the overall processing time to less than 6 minutes per 60 spectra.

After the spectra have been processed – deconvoluted and background corrected – by WinAXIL or WinAXILBatch, calculations must be performed by WinFund. Here, and very much unfortunately some shortcomings of the present form of the program prevent practical fully automatic calculations on a set of spectra. Parameters' setting is totally inadequate for batch calculations. However, after an initial painstaking stage of cumbersome, individual spectrum, parameter setting, automatic calculations can finally be performed on the set. The results have to be manually copied to a worksheet and then sorted or organised in a useful form. Due to the peculiar way in which WinFund outputs the results of its calculations, a routine was developed as an Excel VBA coded macro to automatically sort and organise the WinFund output data, transforming it in numerical values that can be used for further calculations. As a final remark, in spite of all enhancements WinFund is still the bottleneck since it only allows "one file loading at a time" including the specification of the oxides that are to associate to each element present in the sample, element by element, one element at a time. This is a very time consuming task, one that also increases the chance for error enormously.

As a result of the time invested in understanding the software operation, a description of the procedures to be followed, as well as the file format conversion program and the Excel macro enabled worksheet for WinFund data transformation will be made available for the users of ArtTAX equipment at the DCR.

## 5. Conclusions

Considering the comparison of the two types of techniques used in this study, IBA and XRF, it is possible to state that, despite the results obtained with each technique for the archaeological samples showed significant differences between themselves, these differences are consistent with the physical principles of the techniques and to the conservation state of the objects. Although apparently obvious, it is nonetheless worth mentioning that these techniques do not replace each other, except of course in the unlikely case of pristine unaltered homogeneous objects. Instead they do complement, allowing a more complete and encompassing characterisation of the objects under analysis. Stated otherwise the techniques compare well, taking into account their specific probing depths and sensitivity to the state of the surface region of the artefacts and, as such, both are needed, either individually or in combination to the greatest advantage of the analyst.

Nevertheless, there is room for improvements and these may be considered. The geometry and intensity of He flow used in MicroFEx external beam end station should be better defined in order to systematically guarantee a relatively stable Ar free He atmosphere. This is an improvement of major importance since setting the proper He atmosphere enables detection of Na X rays, as recent experiments have shown. And that is by all means a notable achievement, especially in external, non-vacuum environment.

Also, improvement in beam charge monitoring will make the system less sensitive to beam intensity fluctuations contributing to better precision and reliability of the quantification of spectral data.

In what concerns XRF, one major improvement would focus as well on setting a better He atmosphere, one that may also potentiate Na X rays collection (provided that the detector window is not too thick to absorb almost entirely those X rays). Another suggestion is to correctly determine the sample-to-detector real distance and state it to the analysis software, since attenuation of X rays in air is of importance, particularly for the lighter elements, and can significantly affect the results (this is less of a problem in a He pure atmosphere).

In line with the general conclusions stated above, the use of nuclear microprobe based PIXE and PIGE techniques in external analysis, complemented by in air micro-XRF, allowed characterising Roman glasses from different occupation periods of the same settlement, the one of Quinta da Bolacha in the centuries IV to II AD, establishing:

- The elemental compositions and conservation state. Although XRF and IBA techniques produce apparently different sets of results particularly in glasses with significant surface corrosion, due to their different probing depths. Displaying corrosion to varying degrees –

characterised by the low contents of Na and K and the high contents of Mn in clearly identifiable corroded regions – these are, however, glasses with essentially moderate to high Na contents, low in K and Mg, consistent with the general soda-lime-silica compositions known to Roman glasses.

- Natron was used as a source of flux for the production of these glasses.
- Significant levels of Sb and Pb found on one fragment indicate that the opacifying agents used were those characteristic of historical periods until the IV century AD, confirming the time interval of the *villa*'s occupation. No specific elements were found that could be used as fingerprints for attributing a chronology to the objects from revolved contexts. Instead, no distinction between the two sealed contexts could be made based on the bulk composition of the glass fragments collected therefrom, leading to state that most probably manufacture practices of these glasses were common to the contexts.

## References


[1] *A Comparison of the Depth of Analysis of Three Experimental Techniques*, SEM-EDS, PIXE and XRF, http://ion.asu.edu/depth/depth2.htm, 2010.

[2] FERNANDES, P, VILARIGUES, M., ALVES, L. C., SILVA, R. C. da, "Stained glasses from Monastery of Batalha: Non-destructive characterisation", Journal of Cultural Heritage, 9, (2008), 5–9.

[3] LOPES, F., *Uranium Glass in Museum Collections* – Dissertação de Mestrado, DCR, FCT-UNL, 2008.

[4] RUIVO, A., GOMES, C., LIMA, A., BOTELHO, M. L., MELO, R., BELCHIOR, A., MATOS, A. P. de, "Gold nanoparticles in ancient and contemporary ruby glass", Journal of Cultural Heritage, 9, (2008), 134–137.

[5] CRUZ, Mário, *O Vidro Romano no Noroeste Peninsular, Um olhar a partir de* Bracara Augusta*, Volume I, O Vidro Romano no Noroeste Peninsular* – Tese de Doutoramento, Instituto de Ciências Sociais, Universidade do Minho, 2009.

[6] DEGRYSE, P., SCHNEIDER, J., "Pliny the Elder and Sr-Nd isotopes: tracing the provenance of raw materials for Roman glass production", Journal of Archaeological Science 35 (2008) 1993–2000.

[7] Chemistry of Glass, http://www.cmog.org/dynamic.aspx?id=5664&terms=composition%20roman, Corning Museum of Glass, 2011.

[8] SHORTLAND, Andrew, SCHACHNER, Lukas, FREESTONE, Ian, TITE, Michael, "Natron as a flux in the early vitreous materials industry: sources, beginnings and reasons for decline", Journal of Archaeological Science 33 (2006) 521–530.

[9] MIRANDA, J. A., ENCARNAÇÃO, G., Villa *Romana da Quinta da Bolacha, Campanha de Abril/Maio de 1997*, Relatórios-4, Gabinete de Arqueologia Urbana, Associação de Arqueologia da Amadora, 1998.

[10] VAN ESPEN, P., NULENS, H., ADAMS, F., Nucl. Instr. And Meth. 145 (1977) 579.

[11] REIS, M. A., ALVES, L.C., "DATTPIXE, A Computer Package for TTPIXE Data Analysis", Nucl. Instr. and Meth. B68 1-4, (1992), 300–304.

[12] BRONK H, RÖHRS S, BJEOUMIKHOV A, LANGHOFF N, SCHMALZ J, WEDELL R, GORNY HE, HEROLD A, WALDSCHLÄGER U. "ArtTAX – a new mobile spectrometer for energy-dispersive micro X ray fluorescence spectrometry on art and archaeological objects", Fresenius J Anal Chem. 2001 Oct 371(3):307–16.

[13] BRILL, Robert H., *Chemical Analysis of Early Glass – Table of Analysis*, Volume 2, The Corning Museum of Glass, New York; 1999.

[14] Model S-5005 WinAxil X ray Analysis Software, http://www.canberra.com/be/pdf/Cpbsp2m6-WinAxil.pdf,

[15] WOBRAUSCHEK, P., HALMETSCHLAGER, G., ZAMINI, S., JOKUBONIS, C., TRNKA, G., KARWOWSKI, M., "Energy-Dispersive X ray Fluorescence Analysis of Celtic Glasses", X ray Spectrom. 29, (2000), 25–33.

[16] REHREN, Thilo, "Rationales in Old World Base Glass Compositions", Journal of Archaeological Science 27, (2000), 1225–1234.

[17] PAYNTER, S., "Analyses of colourless Roman glass from Binchester, County Durham", Journal of Archaeological Science 33, (2006), 1037–1057.

[18] FREESTONE, I. C. “The Provenance of Ancient Glass through Compositional Analysis”, Mater. Res. Soc. Symp. Proc. Vol. 852 © 2005.

[19] DAVISON, Sandra, *Conservation and Restoration of Glass*, Butterworth-Heinemann, Elsevier Science, Oxford, 2003, ISBN-0-7506-4341-2.

[20] SCHALM, O., PROOST, K., DE VIS, K., CAGNO, S., JANSSENS, K., MEES, F., JACOBS, P., CAEN, J., “Manganese staining of archaeological glass: The characterization of Mn-rich inclusions in leached layers and a hypothesis of its formation”, Archaeometry 53, 1 (2011) 103–122.

[21] VILARIGUES, M., SILVA, R. C. da, "Characterization of potash-glass corrosion in aqueous solution by Ion Beam and IR Spectroscopy", Journal of Non-crystalline Solids, 352, (2006), 5368–5375.